Induced DC Signals due to RF Excitation of the Scanning Tunneling Microscope

Eudean Sun
Department of Electrical Engineering and Computer Science, UC Berkeley
Joonhee Lee
Institute of Physics and Applied Physics, Yonsei University
Xiuwen Tu
Department of Physics, UC Irvine
Dr. Wilson Ho
Department of Physics and Astronomy and Department of Chemistry, UC Irvine

Abstract

Experimental data demonstrated that a direct current (DC) bias between the tip and sample in a scanning tunneling microscope (STM) could be induced by a radio frequency (RF) signal passed through a copper coil placed around the tip of the STM. A resonant response to the RF signal, indicated by an increase in the measured current, was discovered at certain frequencies, including 800MHz, 1.3GHz, and 2.0GHz. This project intended to verify the experimental data by modeling the STM, including the scanner and radiation shields, in Ansoft's High Frequency Structure Simulator (HFSS), and then testing this model for resonance at excitation frequencies from 500MHz to 2GHz in 100MHz steps. Results indicated that resonance is due strongly to the radiation shields (inner and outer) in the model, as the model showed insignificant resonance in the absence of the radiation shields. Further, plots of the electric field across the sample were made in relation to the distance between the tip and sample, varying from 10^{-6} in to 10^{-3} in, which indicated a strong relation between the magnitude of the electric field and the tip-sample distance as well as an extremely strong localization around the tip. Trends seen in results were generally consistent with expectations, but certain inconsistencies did exist in resonant frequencies and electric field magnitudes on the tip, and could be tied to various approximations made in the construction of the model.

Introduction

The Scanning Tunneling Microscope (STM), developed in 1981, is an instrument that allows for the imaging of conductive surfaces at the Angstrom scale (Wiesendanger xv). The STM achieves such high resolution by relying on quantum tunneling, a quantum-mechanical effect whereby a particle may traverse a potential barrier despite having an energy smaller than that of the potential barrier (11). This is possible because of the wave-particle dualism exhibited by particles such as electrons, which allows for a finite probability of finding the particle on the opposite side of a potential barrier despite its lower energy, effectively allowing the particle to tunnel through the potential barrier with a certain probability (11).

In the case of the STM, an electrochemically etched tungsten wire acts as the tip of the microscope, which can be positioned within Angstroms of the conductive sample using piezoelectric drives (91, 101-102). When a DC bias is applied between the tip and sample, electrons can tunnel across the gap between the tip and sample to produce a current called the tunneling current. It can be shown that the tunneling current is exponentially dependent on the width of the potential barrier— $J_T \propto V_T \exp\left(-A\phi^{1/2}s\right)$, where J_T is the tunneling current, V_T the DC bias, $A \approx 1$, ϕ the average barrier height, and s the width of the potential barrier, in this case the distance between the tip and sample (Binnig and Rohrer 237). Thus the tunneling current is highly sensitive to changes in the tip-sample distance, meaning extremely high spatial resolution is possible by using a feedback loop to fix the tunneling current by adjusting the tip position via the aforementioned piezoelectric drives (236). Since the tip of the microscope is electrochemically etched to have a single atom at its apex, the tunneling electrons originate almost exclusively from this point (with negligible contributions from other portions of the tip), meaning the current is localized to the tip apex (Wiesendanger 99). Thus, the tip can be scanned

precisely over the surface of the sample to form a three dimensional image of the surface at the atomic scale—individual atoms can be imaged.

The STM typically relies on a DC bias between tip and sample to produce a tunneling current. However, a DC bias can be produced not only be directly applying a voltage, but also by rectification, the conversion of alternating current into direct current. Experiments involving microwave excitation of the STM have been conducted in the past to study insulators, time-dependent processes at a fixed point, and the nonlinear behavior of the STM (Kochanski 2285; Seifert et al. 379-380). In this experiment, rectification had been observed in the STM when excited by microwave radiation in a copper coil placed coaxially to the tip of the microscope. The atomic-scale rectification experimental setup, show in Fig. 1, involved applying microwave frequencies ranging from 500MHz to 2GHz in 100MHz steps to the copper coil and measuring the resulting current between the tip and sample. Results from this experiment demonstrated the existence of resonance at certain frequencies, indicated by a large amplification gain in the voltage, and formed the basis for the modeling work done in the simulations discussed in this paper. The results from the experimental analysis are shown in Fig. 2, and show resonance at 800MHz, 1.2GHz, 1.3GHz, and 2.0GHz.

Theoretical justification and analysis of this resonance was desired, hence a computer model generated in Ansoft's High Frequency Structure Simulator (HFSS), a finite-element based electromagnetic simulator for high-frequency components, was used to analyze electric fields around the tip and sample to show the relation between the magnitude of the electric field across the tip-sample gap and the frequency of the microwave radiation, as well as the relation between the magnitude of the electric field along the sample and the distance between the tip and the sample. Both of these relationships will highlight the effects of microwave radiation used in

scanning tunneling microscopy and lend support to the existing experimental work in atomic-scale rectification at microwave frequencies.

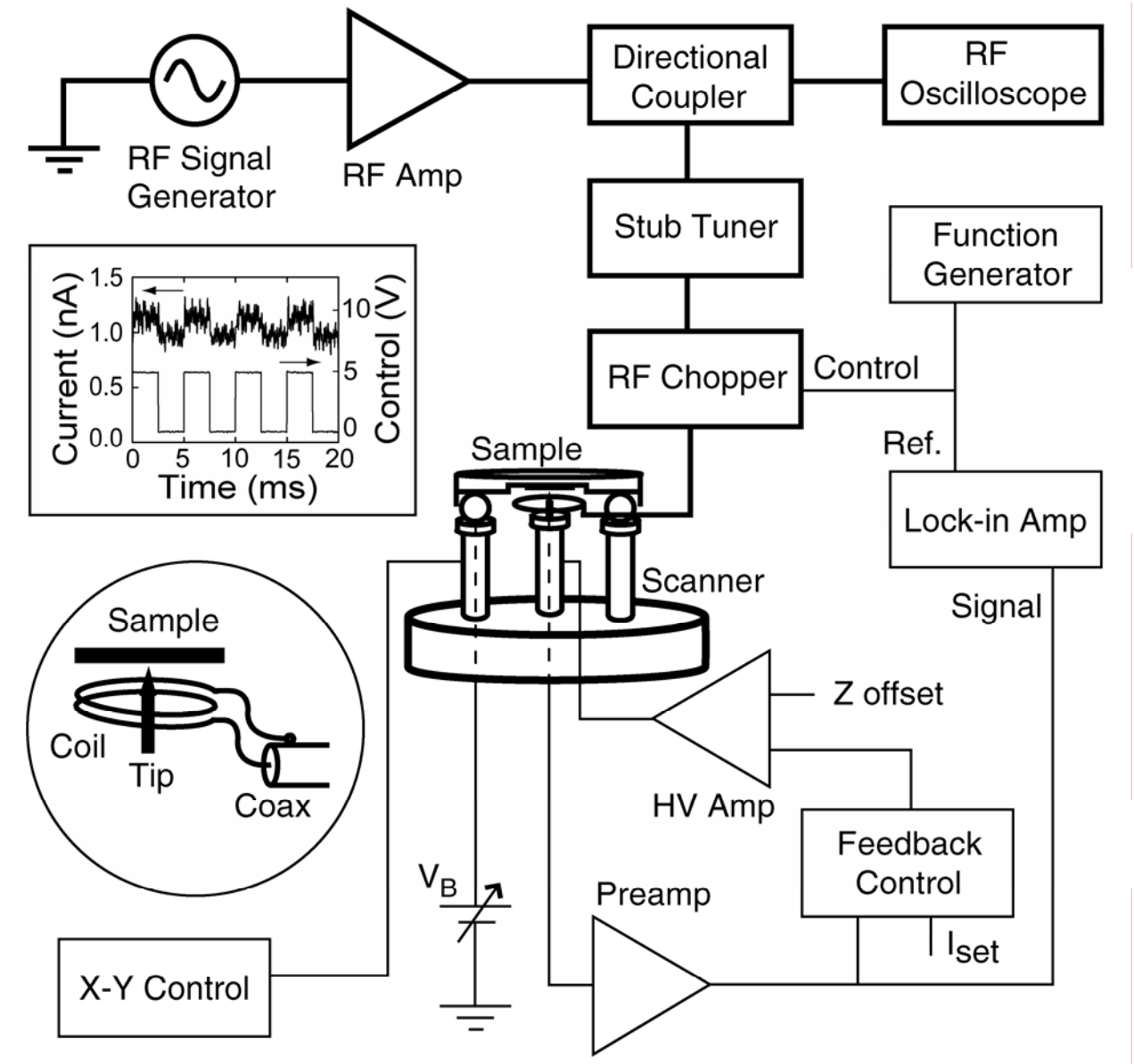

Fig. 1. Schematic of experimental setup.

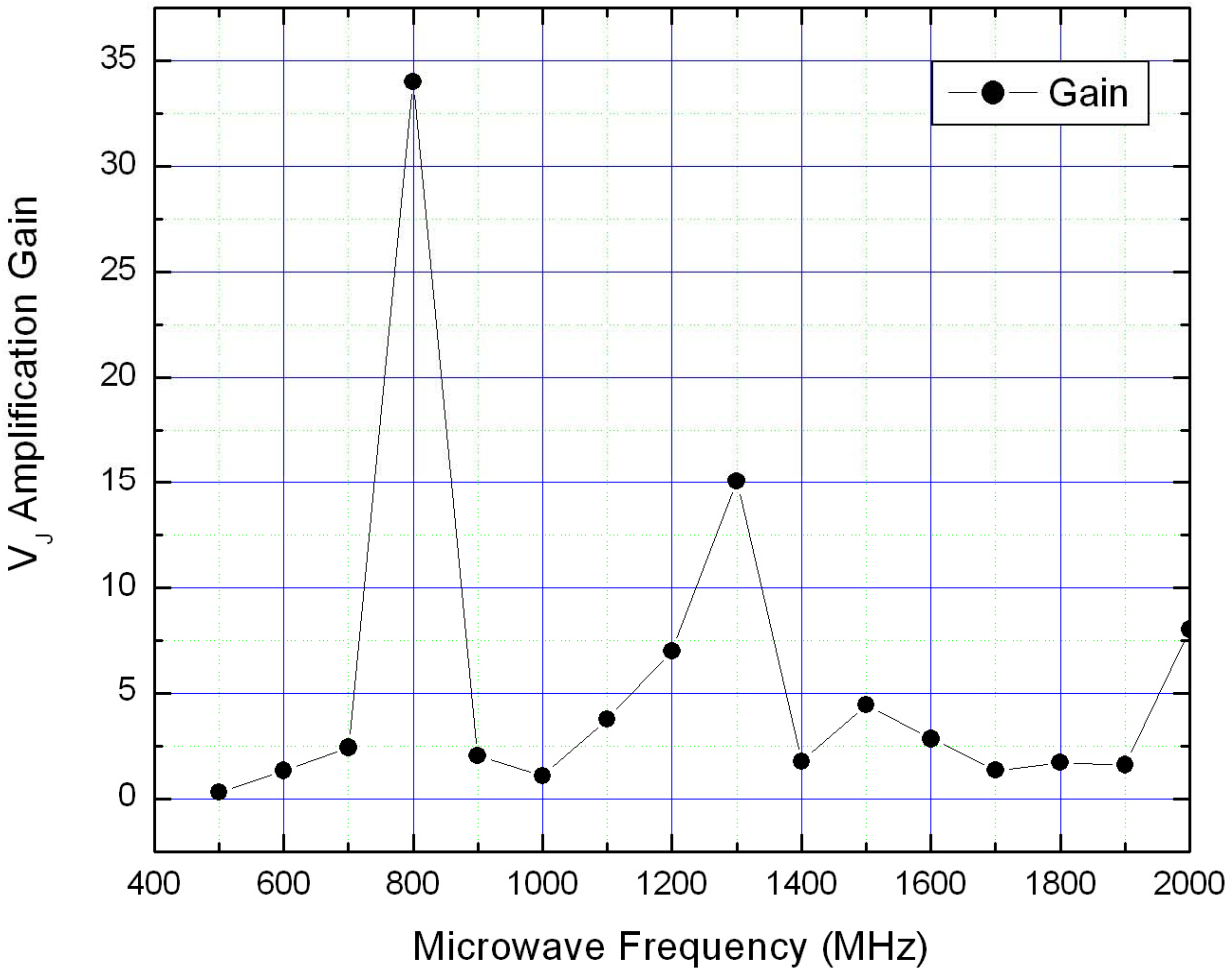

Fig. 2. Experimental results showing resonance at 800MHz, 1.2GHz, 1.3GHz, and 2.0GHz.

Methods and Materials

The first task in running the simulation of the rectification experiment was modeling the geometry of the STM itself. The original modeling work involved converting 2D AutoCAD drawings into 3D models. Due to the limitations of the software and hardware being used, only selective portions of the STM could be modeled; larger bodies such as the vacuum chamber and supporting structures had to be excluded to ensure the model was of a reasonable complexity that could be analyzed in a reasonable amount of time. The original modeling of the components included only the sample holder, piezoelectric drives, tip, inner radiation shield, base plate, RF coil, and crosspiece, although the model would later include more parts. Details such as screw holes were excluded in favor of a simpler design, though all pieces, including window frames and sapphire windows, were modeled accurately otherwise. Initially, the 3D model was built in parts using SolidWorks, constructed within SolidWorks as an assembly file, exported to the IGES model format, and imported into FEMLAB. However, the complexity of the structure resulted in insurmountable problems when it was imported into FEMLAB—separating different bodies into different subdomains was unsuccessful—hence alternative software had to be found. The next attempt at importing the model was with Ansoft's HFSS, and the result proved extremely successful due to HFSS's more flexible and powerful built-in CAD interface. Minor difficulties were encountered in importing the entire assembly as a whole, but separating out certain parts and importing them separately resolved these issues.

Initial modeling of the effects of microwave radiation on the sample was performed after the model was first imported into HFSS. Material properties were assigned appropriately, namely tungsten to the tip, molybdenum to the base plate and sample holder, ceramic to the piezoelectric drives, sapphire to the windows, and copper to the sample, RF coil, inner radiation shield,

window frames, and crosspiece. In addition to these components, a polyline was also drawn from the apex of the tip to the center of the bottom of the sample so the electric field could be plotted in this tip-sample gap region. However, since the software attempts to snap objects separated by extremely small distances, this gap could not be reduced to the desired nanometer size without causing inconsistencies in the results, hence the tip-sample distance had to be set to 10^{-6} in. Although this was certainly a rough approximation, optimetrics analyses performed later would allow for an analysis of trends that would indicate useful information about smaller tip-sample distances as well.

A current excitation of magnitude 2mA was used to excite the coil, modeled as a simple two-turn copper helix, and frequency analysis was performed from 500MHz to 2GHz in 100MHz steps by adding a frequency sweep under the solution setup. Initial results showed resonance at 900MHz, 1.2GHz, and 1.6GHz when the inner radiation shield was included in the model. When the inner radiation shield was excluded, no resonance was shown, demonstrating the preliminary result that the resonance was in fact due to the presence of the radiation shields, a result previously assumed in the experiment but now verified in the simulation. Further, plots of the magnitude of the electric field on the bottom of the sample were made and showed the strong localization of the electric field around the tip apex, another important verification of expected results. The promising nature of the initial data led to the decision to add additional complexity to the model by adding previously ignored details, such as the outer radiation shield, sample holder rails, sample holder grabber (a tab used for positioning the sample holder when inside the chamber), and the coaxial cable bringing the RF signal from the top of the outer radiation shield to the coil. Each component was added incrementally with testing performed after any new part was added to ensure the model was consistent.

While initially simulations were run using the SolidWorks model imported into HFSS, it soon became clear that certain approximations were made in the transition that resulted in dimensions that deviated slightly from the original schematics; these deviations caused problems with overlapping surfaces when new geometries were added. Hence, the model was rebuilt entirely in HFSS using its CAD interface when the outer radiation shield was added. The addition of the remainder of the components was in part to see if the resonance in the model would more closely match the resonance in the experimental data, but this was not the case. However, the addition of the outer shield, coaxial cable, rails, and grabber did result in further changes to the frequency dependence of the electric field; in particular, they enhanced the resonance at 1.4GHz. At this point the geometry of the model was as complete and accurate as planned—no more parts needed to be added, and geometrically the model was consistent with the original experimental setup with the exception of the tip-sample distance, as previously explained—hence, further work went into refining the parameters of the simulation itself. The final model geometry is shown in Fig. 3, along with a comparison to the actual STM used in the experiment.

As previously indicated, the model had been excited by a 2mA current excitation on one end of the RF coil. However, when the coaxial cable was attached, the excitation caused problems as a plot of the current density along the coaxial cable showed it attenuated rapidly along the length of the cable, a clear inconsistency as the high conductivity of copper should show little attenuation along such short distances. Further analysis of the software's documentation indicated that a wave port would produce a better model of current in the coaxial cable; hence, a wave port excitation was placed on the coaxial cable with the integration line running across the dielectric of the cable (Ansoft 6.2-15). This resolved the issue, as plots of the

surface current along the coaxial cable and attached copper coil showed the current was strong within the coil and for the portion of the coaxial cable nearest the end terminated by the coil.

The addition of the extra geometries to the model caused a complication with the model due to the additional complexity: the solution no longer converged below the specified maximum delta S of 0.02 with three solution passes (S refers to the scattering parameters of the model, which HFSS uses in model simulation; delta S is the change in the S between passes). Hence, an additional pass, for a total of four, was added to the solution setup to ensure convergence, resulting in a final delta S of 0.01253. Further, a refined mesh was utilized to enhance the accuracy of the computed electric field on the bottom of the sample. This was achieved by creating a circle on the surface of the sample with a radius of 0.09 inches and assigning length-based and surface approximation mesh operations to the circle, while assigning skin depth based approximations to the sample. Polylines of length 0.18 inches were also plotted on the surface of the sample along the diameter of the circle in increments of 30 degrees, resulting in a total of six different polylines. When solved, the electric field could be plotted along these polylines, which showed the variation of the electric field across the sample. These polylines were used in a parametric optimetrics analysis that tested four different tip-sample distances: 10^{-6} in, 10^{-5} in, 10^{-4} in, and 10^{-3} in. The parametric analysis essentially showed the relation between the tip-sample distance and the magnitude of the electric field across the sample surface, which would allow a reasonable extrapolation of a trend that may shed light on how tip-sample distances down to one nanometer might respond to RF excitation, since such distances could not be accurately modeled in HFSS.

When plotting the electric field on the bottom of the sample with the refined mesh, it was clear that the electric field was actually more localized than originally shown with the coarser

mesh; hence, the radius of the circle used to refine the mesh was reduced to 0.001 inches. Much of the testing performed after this reduction involved discovering the finest mesh applied to the circle that the computer could handle without running out of memory. Unfortunately, the most powerful computer available was limited to 1GB of RAM; hence, mesh refinement could not be performed as much as desired. Values that were finally settled on were 10^{-9} inches for the length-based mesh operation, 0.06 inches for the skin depth mesh operation, and an aspect ratio of 3 under the surface approximation operation with the surface and normal deviations ignored. The mesh produced by these parameters is shown in Fig. 4. Testing indicated that the skin depth mesh operation resulted in the most significant changes in the mesh size; although values down to 10^{-5} inches were tested for the skin depth mesh operation, values that strayed significantly below 0.06 inches always resulted in "out of memory" errors and corrupted computations. Some computations with finer meshes did complete and showed trends more promising than those computations with the coarser mesh—in particular, they showed an order of magnitude difference in the maximum electric field plotted across the sample between the 10^{-6} in and 10^{-5} in tip-sample distances rather than the smaller difference between the two with the final mesh we tested without errors; however, because of the errors reported by the software during the simulation, it is uncertain whether these results were completely reliable.

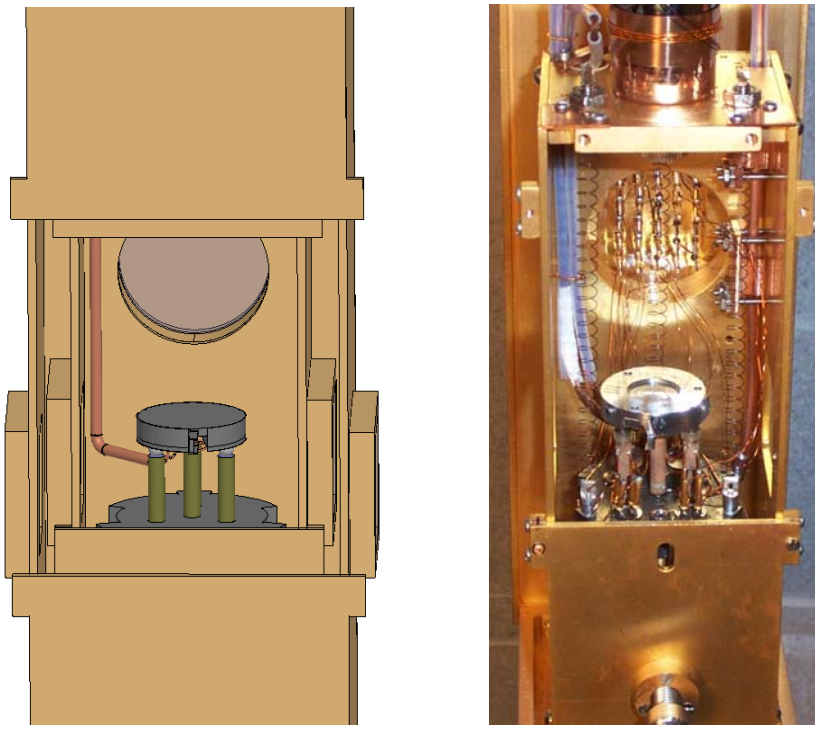

Fig. 3. HFSS model (left) (shield doors hidden) and actual STM (right) (shield doors removed).

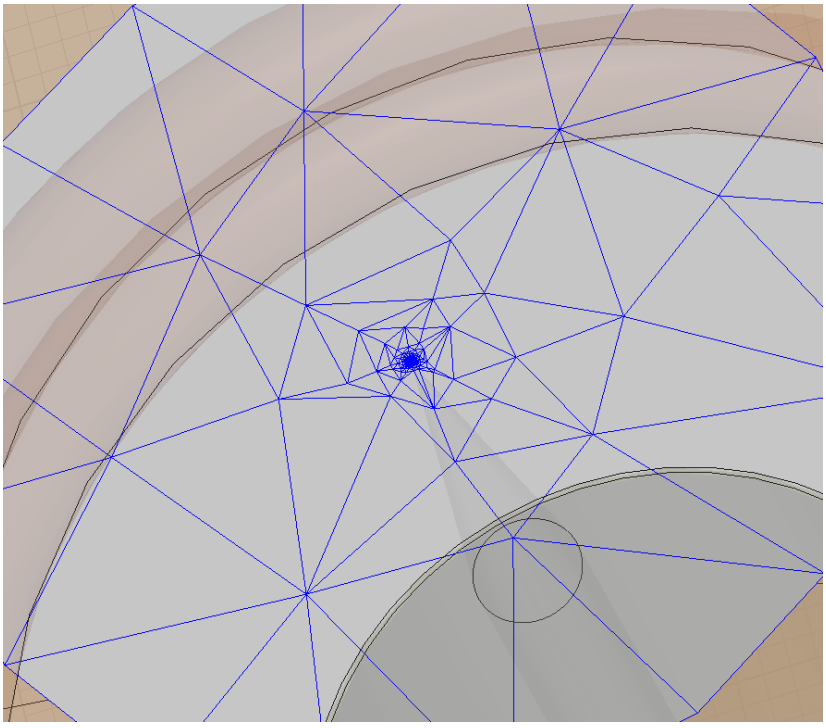

Fig. 4. Plot of mesh on bottom of sample. The outer circle (gray) has radius 0.09 in, while the small blue center, blue due to the extremely refined mesh, is a circle with radius 0.001 in.

Results

The results of the simulation are summarized in Fig. 5 and Fig. 6. Fig. 5 is a plot of the magnitude of the electric field from the tip to the sample versus frequency, produced by the frequency sweep setup. Fig. 6 is a plot of the magnitude of the electric field across the bottom of the sample, with the normalized distance 0.50 in being the center of the sample. The sweep of the normalized distance in Fig. 6 was changed to have 10,000 data points instead of the default 101, 10,000 being the maximum number allowed by the software. The length of the polyline used to plot the fields in Fig. 5 was 10^{-6} in, while the length of the polyline in Fig. 6 was 0.18 in.

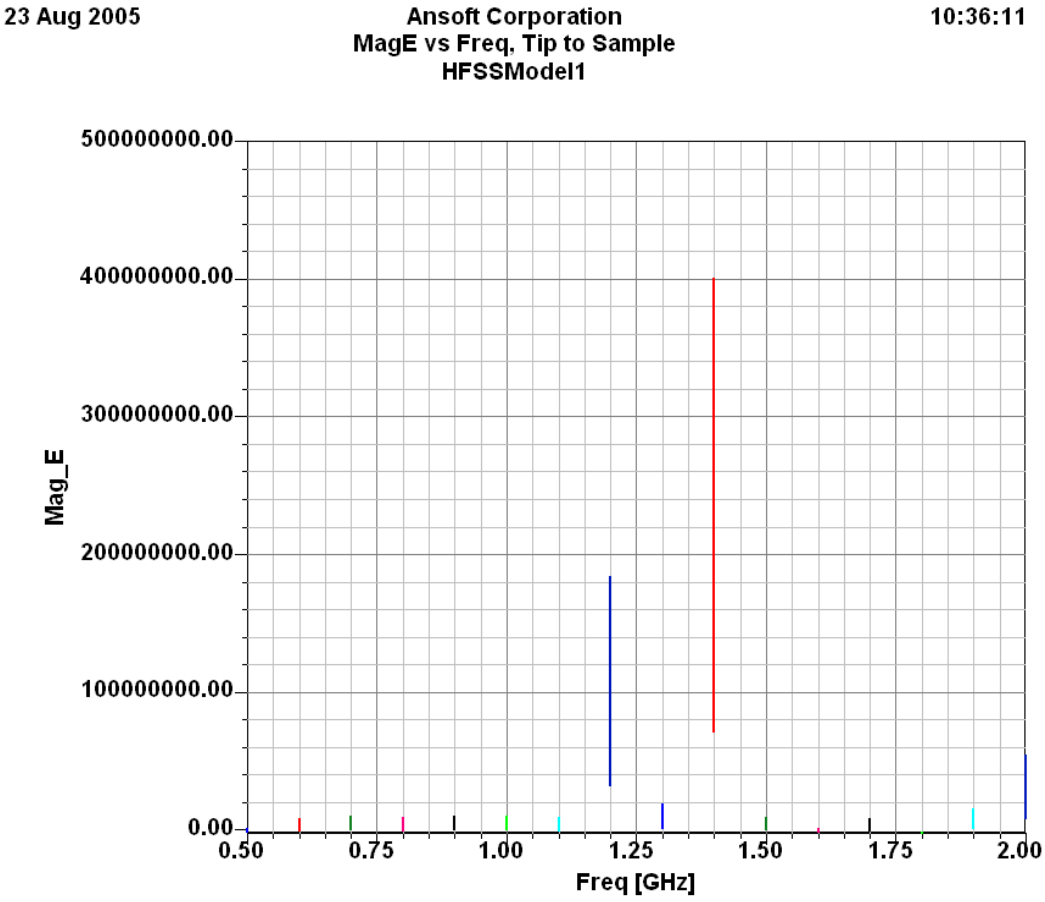

Fig. 5. Magnitude of electric field from tip to sample versus frequency with tip-sample distance 10^{-6} in.

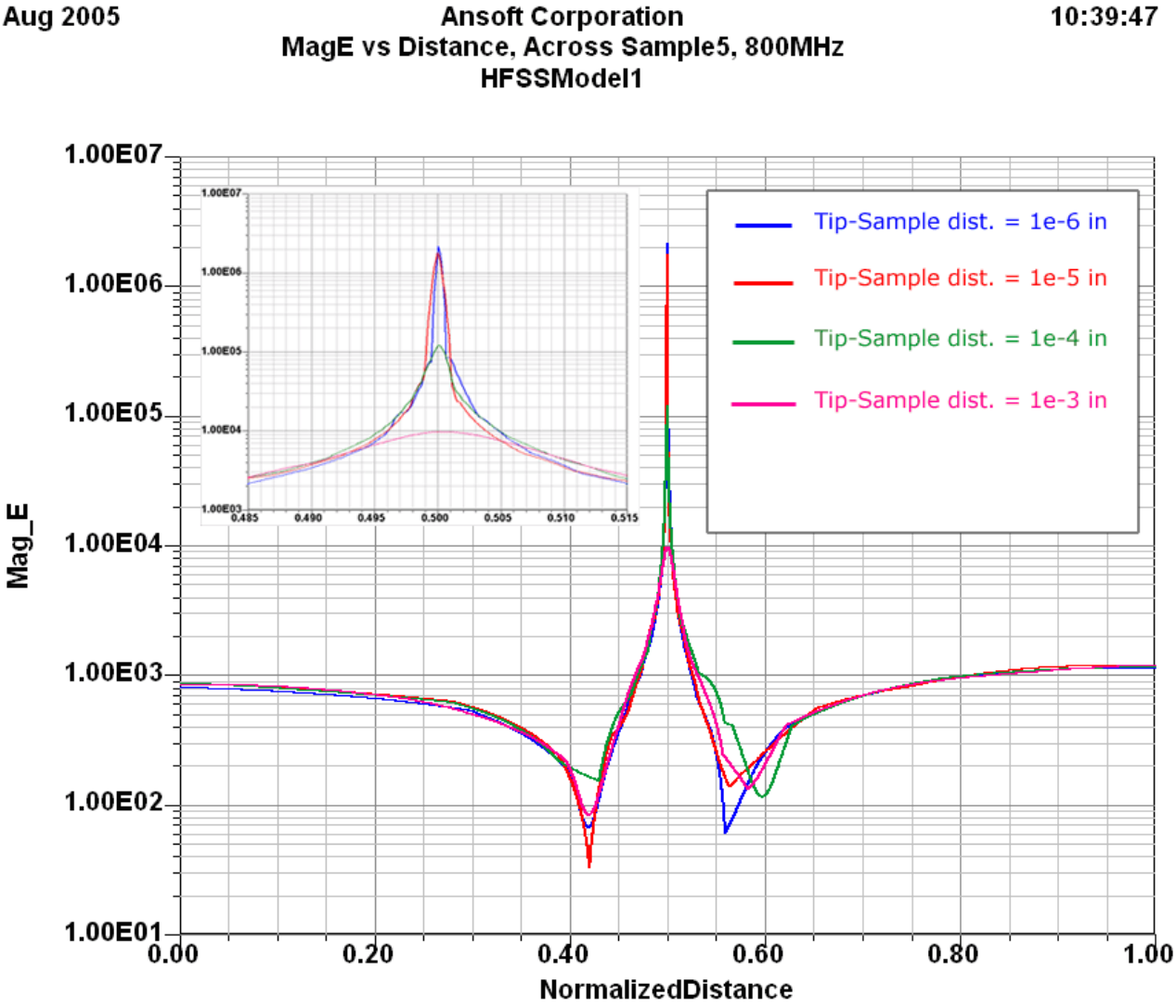

Fig. 6. Magnitude of electric field versus distance across sample. Left inset shows details of E field localization.

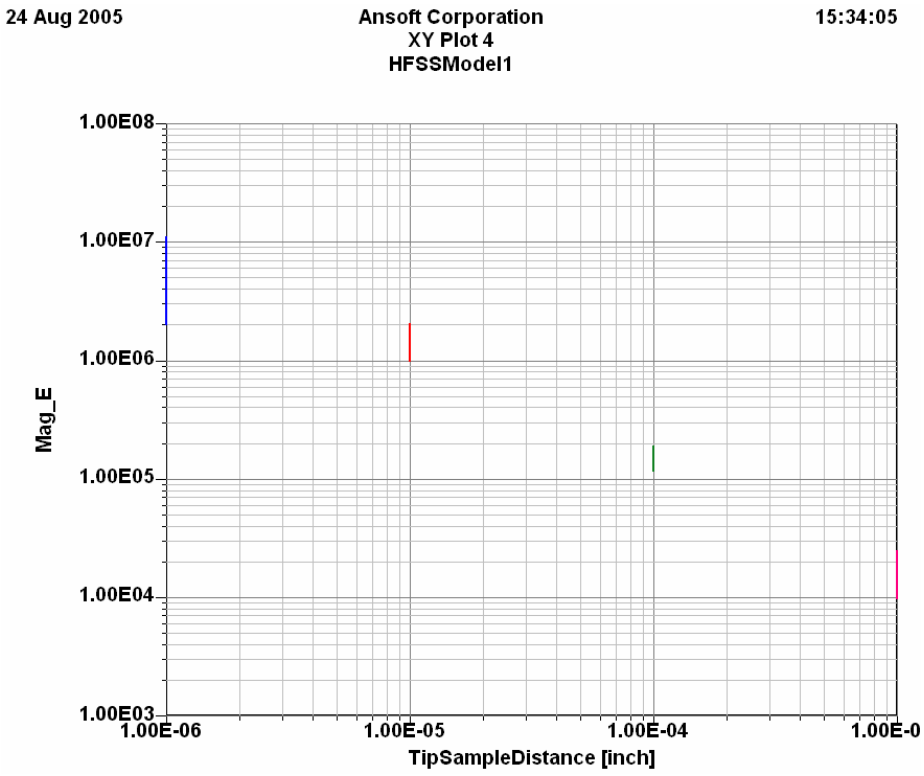

Fig. 7. Magnitude of E field versus tip-sample distance, showing linear relationship.

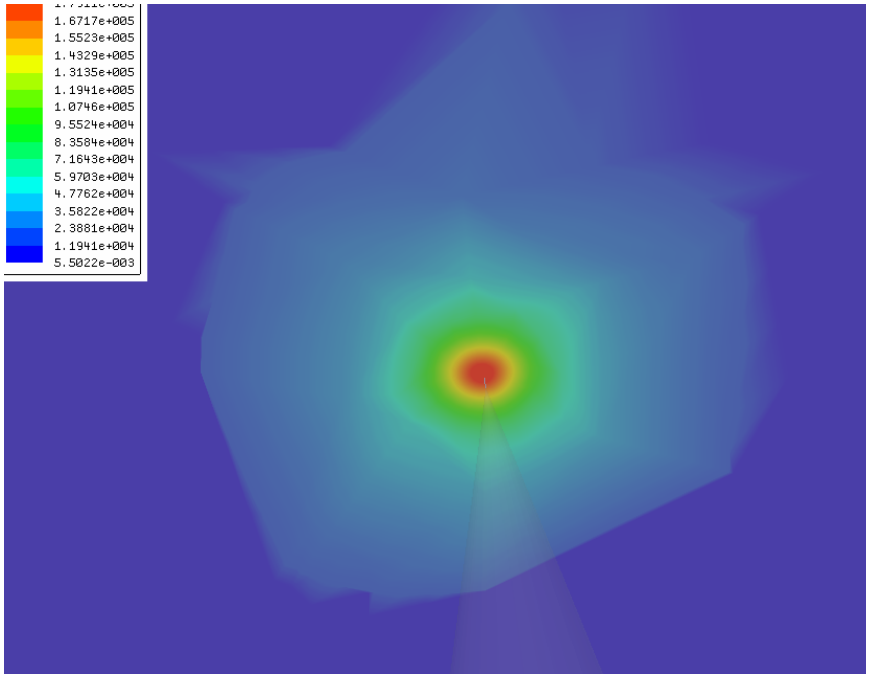

Fig. 8. Localization of electric field with tip-sample distance 10^{-3} in.

Discussion

The results of the frequency analysis conducted with a tip-sample distance of 10^{-6} inches, shown in Fig. 6 show resonance at 1.2GHz, 1.3GHz, and 2GHz, which were predicted by the experimental data gathered prior to the simulation work, though the 1.3GHz resonance is admittedly weak in comparison to the others but clearly stronger than those frequencies showing no resonance. However, they also show clear inconsistencies, the most prominent of which are the lack of strong resonance at 800MHz, which showed the strongest resonance in the experimental data, and the extremely strong resonance at 1.4GHz, which did not show up in the original experimental data.

Although it is unclear exactly where these inconsistencies arose, there are a couple factors that likely influenced the results in subtle or significant ways. The most apparent is the obvious approximations that had to be made in constructing the model. Not every piece could be included—wires, electrodes, springs, external chambers, etc.—hence the model is fundamentally incomplete. While these were expected to have minor effects on the results of the simulation, it cannot be known if indeed they were insignificant details or major factors in the final simulation. Further, as previously indicated, the power of the machine running the simulations also limited the accuracy of the solutions because finer meshes resulted in “out of memory” errors. Every simulation performed while the mesh operations were being adjusted showed different results, even up to the last mesh tested; hence, it is easily foreseeable that a finer mesh could still further change the results of the simulation. In fact, one interesting consequence of the mesh refinement process was watching the localization of the electric field gradually become tighter and tighter as the mesh was refined. In theory, current is tunneling from a single atom on the tip of the STM, meaning the electric field should be extremely localized. With coarser meshes, the field would

appear strong in large areas around the sample center, but with the refined mesh the localization reduced to thousandths of inches and less. This implied that finer meshes could continue to produce significant changes to the solutions of the simulation.

The results of the parametric analysis, shown in Fig. 6, are more straightforward than those of the frequency sweep. It is clear that the magnitude of the electric field on the sample is strongly tied to the distance between the tip and sample, and in the log plot the order of magnitude difference in the electric field between the tip-sample distances shows strongly except between the two smallest distances, which show a smaller difference in electric field. In simulations with finer meshes, the difference in electric field between these two tip-sample distances was much stronger, but as stated before calculations involving the finer mesh tended to result in errors as the machine ran out of memory even with 1GB of physical memory and 4GB of virtual memory, hence they are still inconclusive. It is likely, however, that a finer mesh would alter the results shown here to show a more consistent change in the electric field with respect to the tip-sample distance, but a more powerful computer would be required for such a simulation. Yet another issue with the parametric analysis was the appearance of negative values. Fig. 6 in particular does not demonstrate this anomaly, but on numerous occasions negative values of the electric field would appear in the data—the graph would have, for example, just one point near the peak with a negative value while all others were positive. This was less prevalent as the mesh was refined, hence it is again likely this was due to computation limitations rather than geometry inaccuracies. Finally, it was observed that also on occasion, the peaks of the electric field magnitudes would not line up for the different tip-sample distances, though misalignments were very slight. Again, this was believed to be the result of an imperfect

mesh and a more powerful machine would be able to determine if a finer mesh could eliminate or reduce this inconsistency.

Figure 7 shows the same data as Fig. 6, but plotted in a way to emphasize the linear relationship observed between the magnitude of the electric field between the tip and sample and the tip-sample distance. While the data points corresponding to tip-sample distances of 10^{-6} in are less reliable due to the comparable size of the mesh at such distances, the linear trend it still quite strong and indicates that this trend may continue with smaller tip-sample distances. In relation to observing the behavior of the electric field, the magnitude of the field itself was plotted on the bottom of the sample, as shown in Fig. 8. While originally plots of the E field with a tip-sample distance of 10^{-6} in were used, the fact that the mesh size was on the same order as this feature size resulted in plots that simply followed the shape of the mesh without truly indicating the nature of the E field localization. Taking the tip-sample distance up to 10^{-3} in produced the extremely symmetric plot show in Fig. 8. This localization was expected from the model, and the increasing localization observed with decreasing tip-sample distance was also an expected behavior of the model that was satisfied by the simulation.

Although quantitative data is difficult to gather from the results of the simulation, the observance of trends in general agreement with the results of the experiment remains important in supporting the experimental results. Currently, the model's weakness is in its incompleteness and lack of accuracy, both of which can be resolved given time and resources. Whether these improvements will result in the simulation being consistent with the experiment cannot be said. However, the potential of such a model, if enhanced to generate more accurate data, would be in aiding STM studies by modeling characteristics of the STM in response to high frequency

signals used in RF STM experimentation.

Works Cited

Ansoft Corporation. *User's Guide – High Frequency Structure Simulator*. Pittsburgh: Ansoft Corporation, 2004.

Binnig, Gerd, and Heinrich Rohrer. "Scanning Tunneling Microscopy." *Surface Science* 126 (1983): 236-244.

Kochanski, Greg. "Nonlinear Alternating-Current Tunneling Microscopy." *Physical Review Letters* 62 (1989): 2285-2288.

Seifert, W., *et al*. "Scanning Tunneling Microscopy at Microwave Frequencies." *Ultramicroscopy* 42 (1992): 379-387.

Wiesendanger, Roland. *Scanning Probe Microscopy and Spectroscopy*. Cambridge: Cambridge University Press, 1994.